S. Marimuthu[1]
Laser Processing Research Centre,
School of Mechanical, Aerospace and Civil Engineering,
The University of Manchester,
Manchester M13 9PL, UK

A. Mhich
I. S. Molchan
Corrosion and Protection Centre,
School of Materials,
The University of Manchester,
Manchester M13 9PL, UK

D. Whitehead
Z. B. Wang
e-mail: z.wang@bangor.ac.uk

P. Mativenga
L. Li
Laser Processing Research Centre,
School of Mechanical, Aerospace and Civil Engineering,
The University of Manchester,
Manchester M13 9PL, UK

Z. Liu
Corrosion and Protection Centre,
School of Materials,
The University of Manchester,
Manchester M13 9PL, UK

C. Grafton-Reed
Rolls-Royce plc,
P.O. Box 31,
Derby DE24 8BJ, UK

S. Cheetham
S. Dilworth
BAE Systems (Operations) Limited,
Farnborough,
Hants GU14 6YU, UK

Numerical Simulation of Excimer Laser Cleaning of Film and Particle Contaminants

Laser cleaning is a promising surface preparation technique for applications in high value manufacturing industries. However, understanding the effects of laser processing parameters on various types of contaminants and substrates, is vital to achieve the required cleaning efficacy and quality. In this paper, a two-dimensional transient numerical simulation was carried out to study the material ablation characteristics and substrate thermal effects in laser cleaning of aerospace alloys. Element birth and death method was employed to track the contaminant removal on the surface of the material. The result shows that contaminant ablation increases with laser power and number of pulses. The finite element method (FEM) model is capable enough to predict the optimum number of pulses and laser power required to remove various contaminants. Based on the simulation results, the mechanism of the excimer laser cleaning is proposed. Thus, the use of numerical simulation can be faster and cheaper method of establishing the optimum laser cleaning window and reducing the number of experimental tests.
[DOI: 10.1115/1.4024836]

Keywords: heat transfer, laser cleaning, numerical simulation, titanium alloys, excimer laser

1 Introduction

Cleaning of aerospace components prior to diffusion bonding and electron beam welding is typically carried out using powerful chemicals such as hydrofluoric acid [1]. These techniques require operators to work around hazardous processes and the disposal of waste residues is difficult and expensive. Also, manual cleaning methods tend to be less consistent than automated solutions. To overcome the problems with existing cleaning methods, the use of laser irradiation to clean the material has been explored by many researchers [2–7]. Laser cleaning processes have been found to offer advantages including process automation, remote control, high processing speed per component, dry and importantly, more environmentally friendly processing [1,3,7–9].

During the laser cleaning processes, the thermal effects need to be confined within the contaminants layer [4,5]. Thermal damage on

[1]Present address: School of Mechanical and manufacturing, Loughborough University, UK.

Contributed by the Heat Transfer Division of ASME for publication in the Journal of Heat Transfer. Manuscript received May 29, 2012; final manuscript received May 24, 2013; published online September 27, 2013. Assoc. Editor: Wilson K. S. Chiu.

the base material can affect the performance of the component. Simulation of the laser cleaning process is therefore required not only to understand and control the cleaning process but also to predict the laser process parameters that will give required cleaning quality for different types of contaminants and substrates. Also, numerical simulations are expected to give a better understanding of the embedded phenomena and removal mechanism of the contaminants.

Mathematical models have been developed in the past to study the laser interaction and removal of contaminants during laser cleaning process. Most of these models are based on laser ablation of thick materials in the order of at least few micrometers. Song [10] developed a one-dimensional laser cleaning model based on heat conduction equations and showed that the laser cleaning force per unit area increases with increases in laser power and number of pulses. This model was focused primarily on removing particles from magnetic disk. Zhou [11] simulated the laser ablative cleaning of Zn-coated carbon steel using one-dimensional formulation. They formulated the relationship between laser power and ablation rate which was in good agreement with the experiment. A two layer (stainless steel substrate layer and oxide layer) based laser cleaning model was developed and validated by Furukawa [12]. They used one-dimensional formulation with melting and vaporization effects to find the ablation rates for various laser intensity and laser beam angles. A one-dimensional and two-dimensional model for laser ablative cleaning of copper oxide from pure copper substrate have been developed by Zhang [13]. They concluded that the results of the two-dimensional model was close to the experimental results and also showed that a minor increase of number of pulses than optimal values did damage the substrate. Tosto [14] described a three dimensional analytical model to find the ablation rate induced by laser irradiation. Oliveira [15,16] formulated a two-dimensional FEM model based on pure conduction to study the vaporization effect of Al_2O_3–TiC by KrF and Nd:YAG laser irradiation. Furthermore, their model predicted very high temperatures on the material surface which results in high ablation rate. Mullenix and Povitsky [17] compared one and two-dimensional laser ablation models, in which the heat transfer mechanism within the target is modeled as conduction and the material removal is modeled as sublimation, with surface absorption of the laser. Numerical simulation on laser ablation of carbon and the effects of plasma plume shielding was studied extensively by Zinovik and Povitsky [18]. Sinha [19] used a two-dimensional finite difference model based on conduction equations to find the temperature distribution, melt depth and evaporation rate for Nd:YAG laser ablation of fuel pellets. Khalil [20] presented a two-dimensional FEM model to simulate the pulsed laser ablation of stainless steel material.

Most of the models discussed in the past are based on fixed grid methods, in which there is limited chance to track the surface geometry changes as a result of laser ablation. In laser cleaning process the surface geometry changes with pulses and a robust model is still lacking to track the geometric variation or progress of the laser cleaning process. Also, the laser cleaning model should be capable of addressing the geometry and boundary nonlinearity's that happen during the transient laser cleaning processes.

The present study involves two-dimensional FEM modeling of the excimer laser cleaning of engineering materials with various contaminants for the investigation of the effects of laser parameters on cleaning efficacy and the ways of controlling thermal damages to the substrates. The numerical model corresponds to excimer laser cleaning process with pulse duration of 20 ns and beam size of 1 cm by 1 cm over the substrate. In the first part, thermal analysis of excimer laser cleaning over a flat plate with film contaminants is considered. In the second part of the study, laser cleaning of spherical particles was considered. The FEM analysis was carried out using ANSYS software. The experimental results obtained with a 248 nm excimer laser, was used to validate the FEM results obtained under similar processing parameters.

2 Finite Element Model

The target of laser ablation was represented by a mesh of finite elements that changes over time so as to simulate the transient thermal profiles and transient ablation characteristics. The finite element programming language ANSYS with user programming [21] was used to perform the analysis. The following are the specific assumptions considered in the current analysis:

(a) the excimer laser cleaning is performed at a relatively low power density [7] and frequency (maximum of 200 Hz), so the effects of plasma plume, gas dynamics and shock waves during laser irradiation process were insignificant [22] and assumed negligible in the model.
(b) the size of the computational domain was designated to study the material removal characteristic at the ablated region and not to predict the bulk substrate temperature.
(c) the removal of all the contaminant material is a consequence of vaporization due to high temperature [17].
(d) the mode of heat transfer inside the substrate and contaminant is through conduction [17,23].
(e) at the substrate–contaminant interface, the laser beam was assumed to reflect and regarded as a surface source [4,5].

A pure thermal conduction model was reported to be applicable in laser irradiation if the pulse duration (p_d) is in the range of $10^{-12} \leq p_d \leq 10^{-9}$ s [23] which is valid for the excimer laser ablation process. Previous experimental studies have also shown that at optimal ranges, the excimer laser cleaning process was primarily driven by thermal effects [24,25]. Titanium alloy substrates, with four different contaminants that are commonly found in aerospace industrial environment were considered for this study. The material properties used for the substrate was adapted from Weast [26] and the material properties used for the contaminants is shown in Table 1. The material properties for the contaminants (obtained from the manufacturer's data sheet), and the substrate [26] are listed in Table 1 and Table 2.

Figure 1(*a*) shows the domain used in the modeling of thin film contaminant layer. To moderate the computational time, a reduced domain consisting of a small region (3 μm in height and 5 μm in length) was considered for the analysis. As the heat penetration depth into the titanium alloy with the excimer laser processing is only about 430 nm [27], this smaller domain should be sufficient to capture the thermal effects at the vicinity of ablated region in excimer laser cleaning process. Also, adiabatic boundary condition was considered on the all three sides to simulate a semi-infinite condition. The contaminant layer was set as 300 nm thick on the titanium substrate. This was in line with the experimental

Table 1 Material property of the contaminants

Contaminant properties	Hydraulic oil	Silicone grease	Yttria	Magnesium oxide
Density (kg/m^3)	872	1000	5010	3580
Specific heat (J/kg K)	1800	1200	456	877
Conductivity (W/m K)	0.15	3.0	27	42
Latent heat of vaporization (J/Kg)	745×10^3	960×10^3	4135×10^3	4680×10^3
Boiling/decomposition temperature (K)	626	913	4573	3173
Beer–Lambert penetration depth (μm)	0.36	0.11	—	—

Table 2 Material property of the substrate

Properties	Values
Density (kg/m^3)	4430
Specific heat capacity (J/kg K)	610
Thermal conductivity (W/m K)	21
Melting temperature (K)	1928
Boiling temperature (K)	3315
Latent heat of melting (J/Kg)	296×10^3
Latent heat of vaporization (J/Kg)	8880×10^3

glow discharge optical emission spectroscopy measurement. Over the top surface of the domain, a stationary, uniform laser beam of size 2 μm was considered.

Variable meshes, with very fine meshes at the contaminant and course meshes expanding gradually away from the top were used to obtain improved accuracy with the limited elements. The use of a thinner mesh in the upper part of the substrate allows a more precise estimation of the material removal. Figure 1(*b*) shows a small portion of the finite element mesh (case-I) with 94,500 quadrilateral elements that was used for the FEM analysis. The latter part of the simulation (case-II) deals with the FEM analysis of laser cleaning of particles.

The transient thermal problem was solved by varying boundary conditions and time steps according to the laser pulse shape and number of pulses. The time steps are linked to each other by using the output of time step, *ts*, as the initial condition for time step ($ts + 1$). The workpiece was initially set at a room temperature of 298 K. The pulse length (P_L) in excimer laser was 20 ns and the laser off time (T_p) between each pulse was calculated using Eq. (1)

$$T_p = (\text{frequency})^{-1} - P_L \tag{1}$$

The governing equations for two-dimensional transient heat conduction can be expressed by Eqs. (2) and (3) for the contaminants and the substrate, respectively:

Contaminants

$$(\rho c)_c \frac{\partial T(n,t)}{\partial t} = \frac{\partial}{\partial n}\left[k_f \frac{\partial T(n,t)}{\partial n}\right] + S_c \tag{2}$$

Substrate

$$(\rho c)_s \frac{\partial T(n,t)}{\partial t} = \frac{\partial}{\partial n}\left[k_s \frac{\partial T(n,t)}{\partial n}\right] + S_s \tag{3}$$

Subscripts *s* and *c* represent the substrate and contaminants, respectively. The parameters n, T, t, k, ρ, c, S_c and S_s denote normal vector, temperature, time, thermal conductivity, density, specific heat, heat source absorbed by the contaminants and the heat source absorbed by the substrate.

These heat sources are such that S_c is applied on all the elements defining the contaminants while S_s is applied only on those elements of the substrate that are in contact with the contaminants. For a laser peak power of, P and a Beer–Lambert absorption depth, δ_{BL} the respective definitions of these heat sources are given by Eqs. (4) and (5).

$$S_c = \frac{P(1 - R_c)}{\delta_{BL}} e^{-\frac{y}{\delta_{BL}}} \tag{4}$$

$$S_s = \frac{P(1 - R_s) e^{-\frac{y}{\delta_{BL}}}}{\text{Thickness of first cell}} \tag{5}$$

R_c and R_s are the reflectivity of contaminates and source, respectively, which was experimentally estimated using an Ocean Optics SD2000 spectrometer. The reflectivity of substrate, yttria, magnesium oxide, silicone grease and hydraulic oil at the wavelength involved was found to be 0.45, 0.24, 0.26, 0.06, and 0.08, respectively.

Showing the intensities of both heat sources to be a function of the parameter *y*, which represents distance measured from the surface of the contaminants to any depth in its thickness. For the contaminants the Beer–Lambert absorption depth, δ_{BL} was experimentally evaluated [5] and reported in Table 1.

During the simulation, if the temperature of an element is higher than the melting temperature (*Tm*) at the end of a particular step, melting is assumed to have occurred and the latent heat of melting (*Lm*) is taken into account in the calculation. Similarly, material removal is assumed to occur when the temperature of the elements is higher than the decomposition/boiling temperatures of the material. The "element death" methodology (available in ANSYS) was used for simulating the material removal. Such an element was considered to be dead, with insignificant effect in subsequent analysis. The heat sources S_c and S_s are assumed to be a top-hat distribution and are applied as a volumetric heat source. The applied heat source region was not predetermined and was calculated by the program in a transient manner according to the shape of the ablated profile as elucidated in Fig. 2. During the initial start of the simulation, the heat source is applied over the full region (Fig. 2(*a*)). As the simulation proceeds, due to the material removal the contaminants surface geometry changes, and subsequently, the laser beam heat source geometry also changes as shown in Fig. 2(*b*).

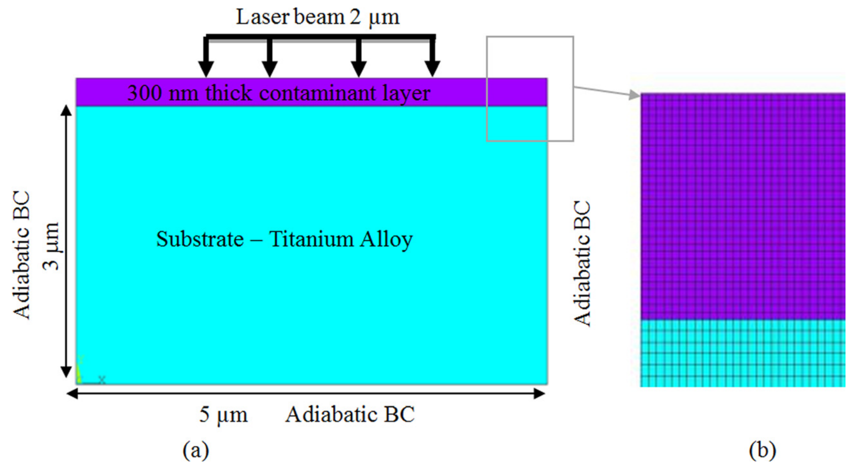

Fig. 1 Model domain and FEM mesh used for laser cleaning of flat contaminant layer (BC—means "boundary constraint")

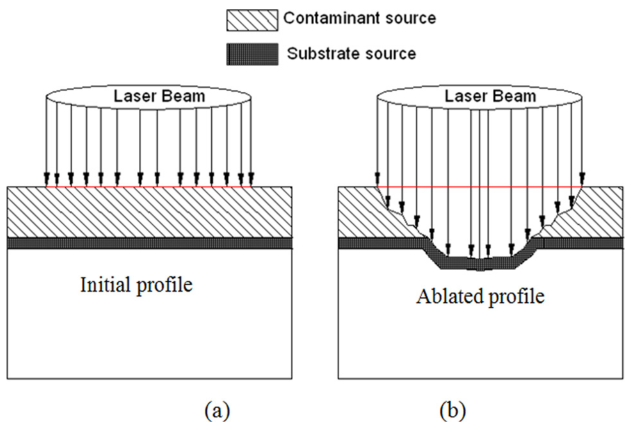

Fig. 2 Strategy used for applying surface heat sources for various surface profiles

The initial conditions for the thermal analysis were taken as

$$T(n,0) = 298\ \text{K} \quad \text{and} \quad T(\infty,t) = 298\ \text{K} \tag{6}$$

Heat loss due to convection was considered in the top surface exposed to atmosphere as

$$k\frac{\partial T}{\partial n} = -h(T_s - T_\infty) \tag{7}$$

Here T_s, T_∞, and h denote cell temperature, ambient temperature, and heat transfer co-efficient, respectively.

A heat transfer co-efficient [28] of 10 W/m^2 K was used in the FEM analysis. The procedure employed in this study for solving the heat transfer equations is given as a flow chart shown in Fig. 3. As indicated in the flow chart, the simulation process occurs in four steps: The first step includes the model generation phase and specifying the respective boundary conditions. The second step corresponds to laser pulse interaction and material removal. Then, the third step is for the cooling phase during the time between two consecutive laser pulses and finally step four involves postprocessing of the results and generating the outputs results.

3 Results

3.1 Laser Cleaning of a Contaminant Film. To understand the effect of laser process parameter on cleaning efficiency, a parametric study was conducted for various laser peak powers, number of laser pulses, laser beam angle and contaminant types. Experimental findings showed that these parameters, i.e., laser peak power, number of pulses, type of contaminants, and the laser beam incident angle were most significant parameters in laser cleaning.

The effect of laser peak power on the temperature changes and its subsequent material removal is shown in the Fig. 4 for the titanium alloy substrate and yttria (yttrium oxide) contaminants. Figure 4 is plotted at the end of 20th laser pulse (includes the laser off time between pulses) before the material cools down to room

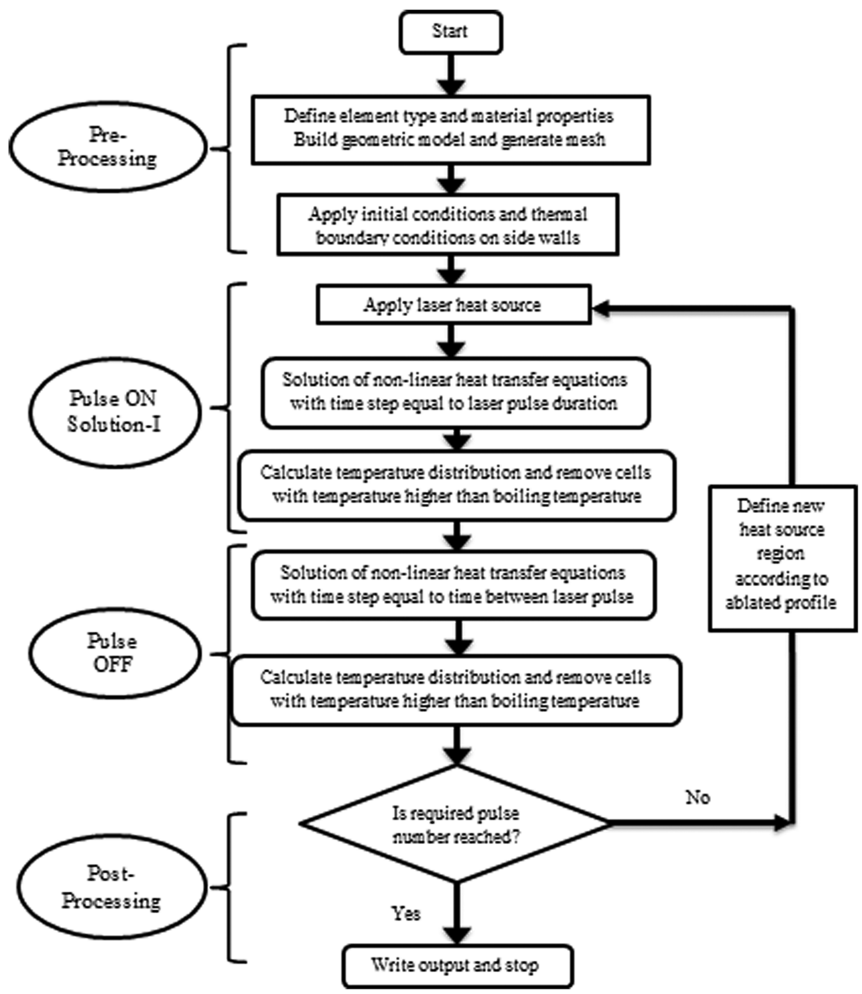

Fig. 3 Flowchart explaining the analysis steps

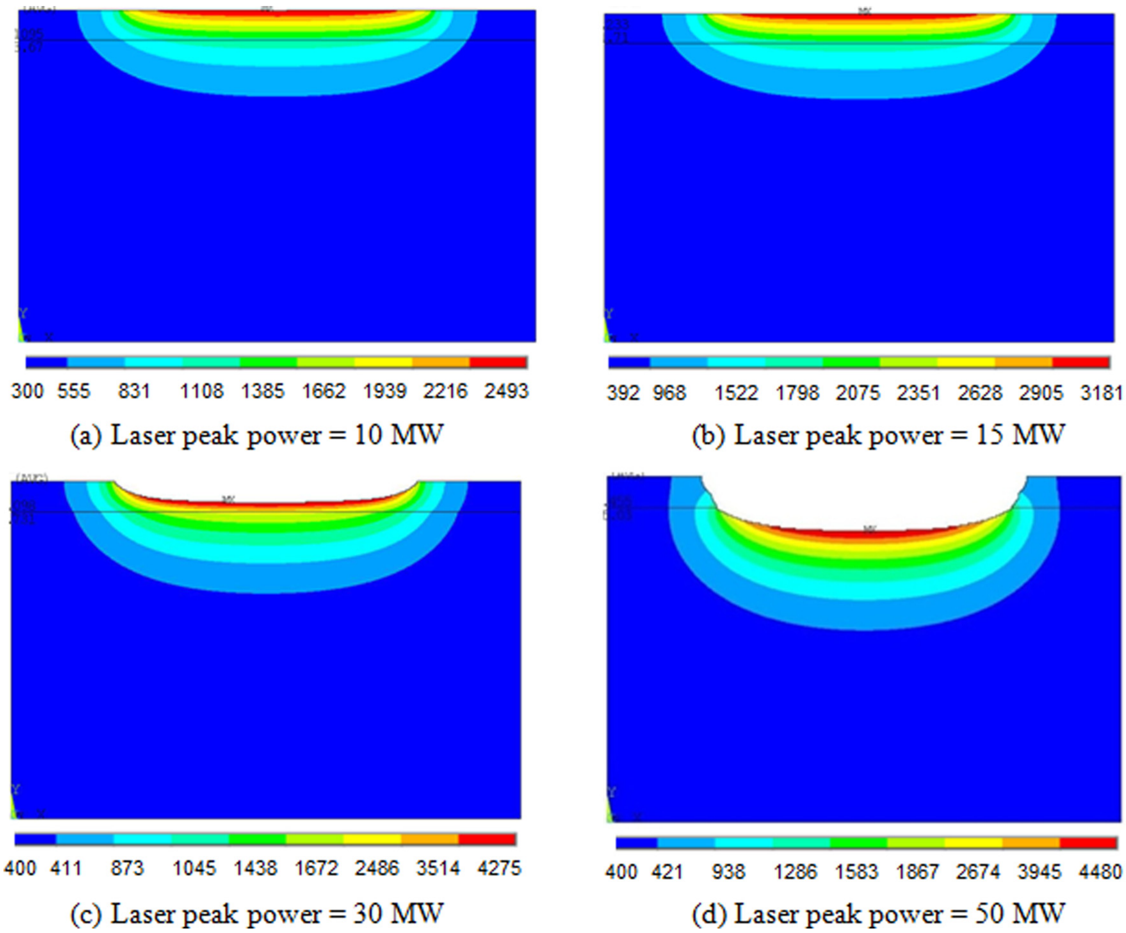

Fig. 4 Effect of laser peak power on temperature profile (K) and contaminant removal (contaminant type = yttria, number of pulse = 20)

temperature. As shown in the figure the minimum threshold required for effective removal of yttria is close to 30 MW and any laser peak power value less than this fails to create significant contaminant removal. Also noted from this figure is that with further increase in laser peak power (50 MW), the substrate material starts to ablate even with 20 number of pulses.

Figure 5 shows the variation of maximum and minimum temperatures recorded on the substrate surface with Yttria as the contaminant layer. As noted from the figure, high peak temperatures are observed during the pulse-on period (20 ns) and the temperature drops drastically close to the ambient temperature before the start of the next laser pulse. The surface temperature keeps on increasing with the increase in the number of pulses per location irrespective of the laser power values. The accumulated bulk temperature (minimum temperature) for laser peak power of 20 MW is close to 850 K, whereas for a laser peak power of 40 MW it reaches up to 1100 K. This is a critical phenomenon to be noted, as high bulk temperature may cause thermal cracking and material oxidation of the substrate material. Although, the maximum temperature is high, due to the short interaction time (20 ns) the bulk material temperature has not increased significantly so as to cause any metallurgical changes.

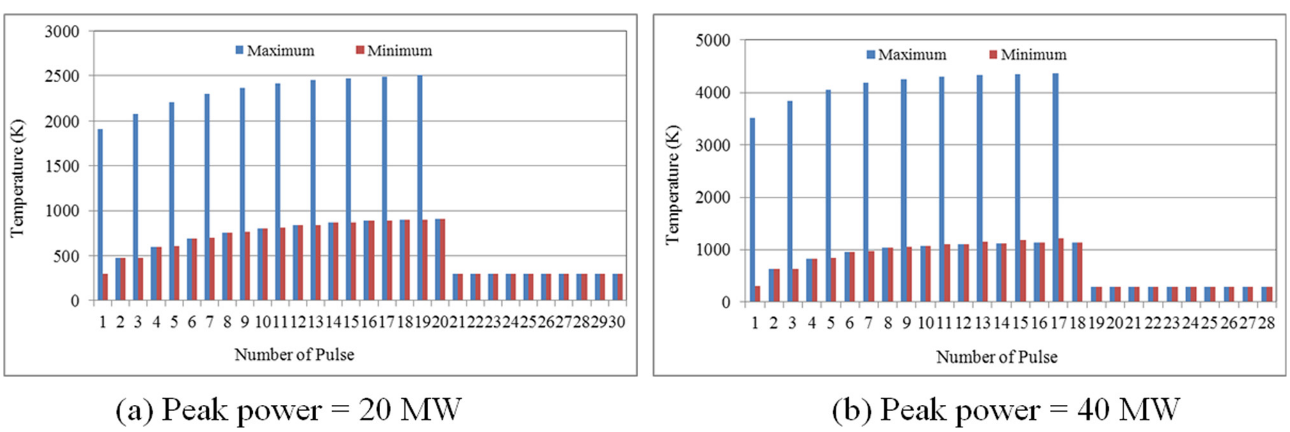

Fig. 5 Variation of maximum and minimum temperatures for various number of pulse (contaminant type = yttria)

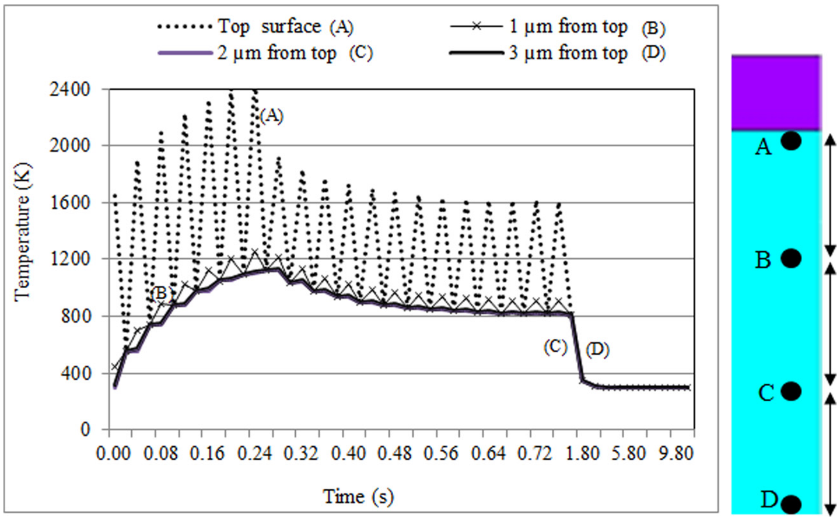

Fig. 6 Variation of temperature with depth and time (laser peak power = 30 MW, contaminant type = magnesium oxide, number of pulse = 20)

Figure 6 shows the variation of temperatures with depth and time for a laser peak power of 30 MW and magnesium oxide contaminants. With magnesium oxide contaminants, the temperature of the substrate material increases with an increase in the number of pulses and once the contaminants are fully removed there is a rapid reduction of temperature. This reduction is due to the immense change of material properties between the Ti alloy substrate and magnesium oxide contaminant, which eventually decreases the temperature for a small period and then again the substrate temperature increases with an increase in number of pulses. As indicated from Fig. 6, the temperature in the bulk material drastically decreases with distance from the top. The thermal diffusion time of the substrate material is less than the excimer laser interaction time which restricts the accumulation of high temperatures in the bulk substrate material.

The variation of substrate surface temperature for 50 pulses for the removal of yttria is shown in Fig. 7. As seen, the substrate temperature increases rapidly for the first few pulses, and then increases slowly with further increase in number of laser pulses. The initial increase in substrate temperature corresponds to the time required for the material temperature to reach quasi-steady state temperature. Another phenomenon observed is that the bulk temperature comes back to the ambient room temperature in less than one microsecond, which is attributed to the short pulse duration of the excimer laser.

Figure 8 shows the contaminant removal characteristics and thermal profile for laser peak power of 15 MW and the number of pulse of 20. As seen from the figure, complete removal is noticed with hydraulic oil and grease contaminants, whereas there was no removal of yttria and magnesium oxide contaminants. The temperature produced for a laser peak power of 15 MW and 20 pulses is not sufficient to vaporize yttria and magnesium oxide contaminants. Also, in case of hydraulic oil removal, due to its low decomposition temperature, the contaminate absorbs heat from the substrate and decomposes even in regions where the laser heat source was not applied. As expected, at the end of 20 pulses the substrate temperature is higher for the substrate with hydrocarbon contaminants (hydraulic oil and grease), whereas the substrate with oxide contaminants shows lower temperatures, as most of the laser heat is used only to raise the temperatures of the contaminants. This is in line with the findings in Fig. 4 in which, a peak power of 40 MW is required to effectively remove yttria and magnesium oxide contaminants.

The effect of laser beam incident angle on the temperature characteristics on the substrate surface for laser peak power of 15 MW, 20 laser pulse and with hydraulic oil contaminant is shown in Fig. 9. The change in laser beam angle changes the beam intensity distribution and size and eventually the number of pulse per position (when the beam is moving). With an increase in beam angle, the beam size over the substrate increases, this subsequently reduces the heat source intensity on the material. As seen from the Fig. 9, with increase in laser beam angle the maximum surface temperature and the minimum bulk temperature reduce. This effect is found for laser beam angles more than 15 deg. Another fact is that the temperature produced with a high beam angle is sufficient to remove the hydrocarbon (hydraulic oil and grease) based contaminants, so increasing the beam angle, which subsequently increases the beam size, is an option to achieve high cleaning efficiency and for removal of contaminants over complex component geometry including slots and corners.

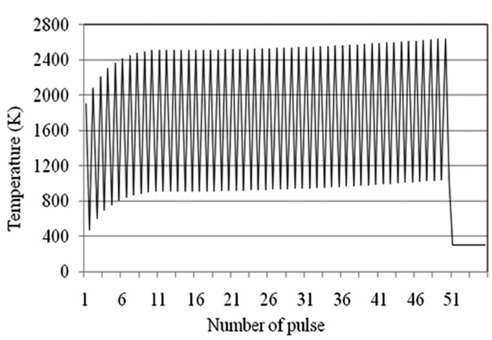

Fig. 7 Variation of temperature with number of pulse (laser peak power = 15 MW, contaminant type = yttria)

3.2 Laser Cleaning of Film Contaminant Layer With Particles. In most industrial components, the contaminants are not only as a thin layer of film, but many particles are also found. The second part of the simulation is focused on laser cleaning of particles within the contaminant layer. Figure 10(*a*) shows the domain used for this analysis. The model consists of 3 μm height by 5 μm length titanium alloy substrate with 300 nm thick grease contaminant layer and 1.2 μm diameter yttria particle. A small portion of the mesh used for this analysis is shown in Fig. 10(*b*). The FEM model is based on same two-dimensional formulation discussed in Sec. 2 of this paper.

Figure 11 shows the temperature and ablation characteristics for various power levels and with 20 laser pulses over a grease

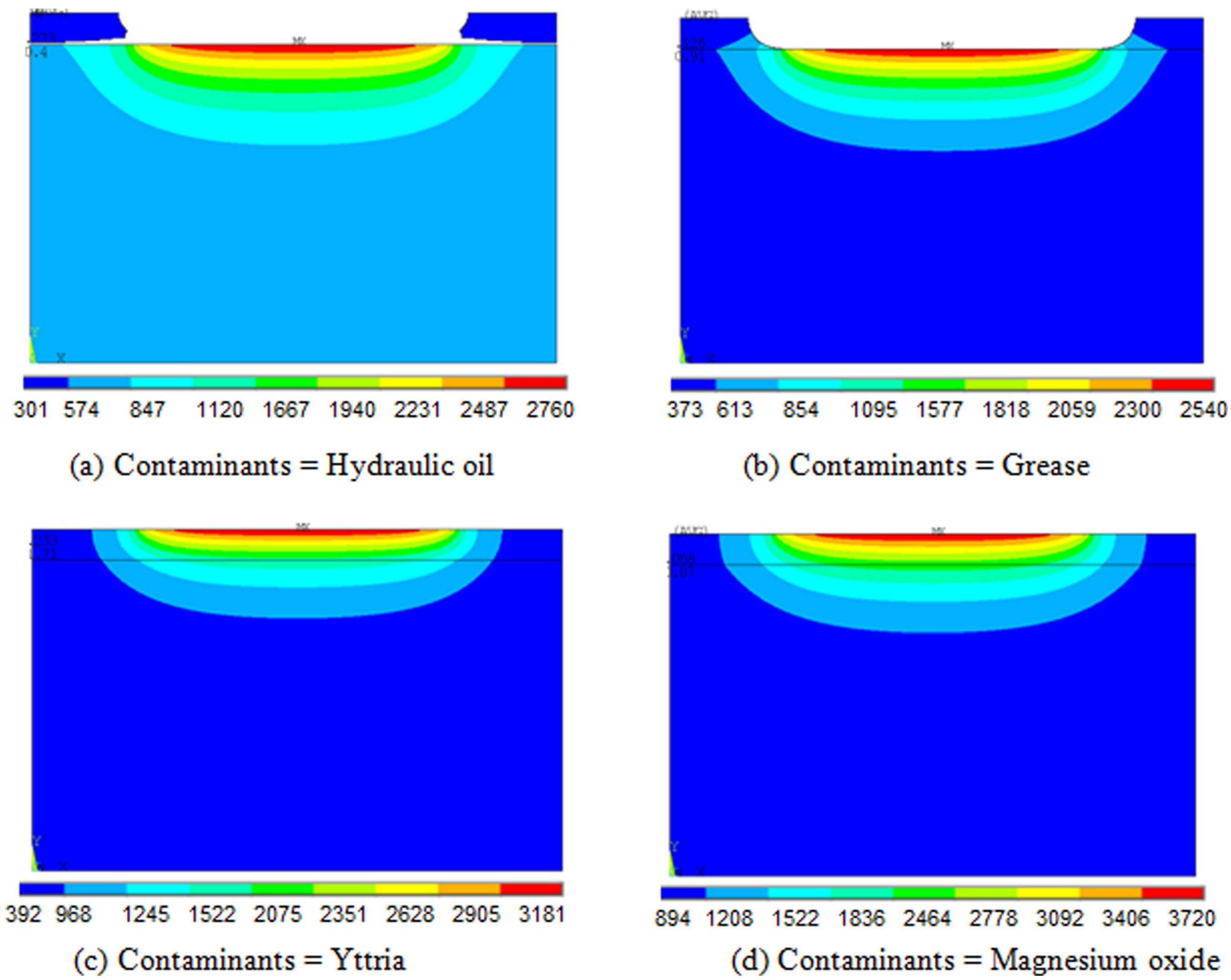

Fig. 8 Effect of contaminant types on temperature profile (K) and contaminant removal (laser peak power = 15 MW, number of pulse = 20)

contaminant layer and an yttria particle. As seen, the simulation shows a process of the ablation characteristic noticed in excimer laser cleaning. With 20 laser pulses, effective removal of grease flat layer contaminants is found for a peak power value higher than 15 MW. The ablation of yttria particles start with peak power of 30 MW and full removal is found only at a peak power of 50 MW for 20 pulses. Although full ablation of yttria particles is noticed for high peak power, it also ablates the titanium substrate as noticed from Fig. 11(*d*).

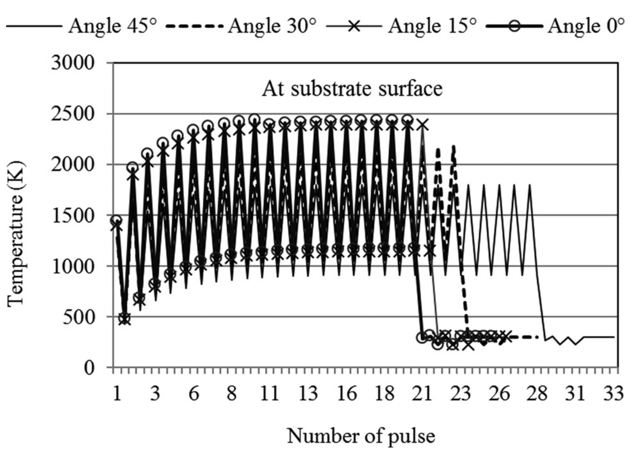

Fig. 9 Variation of temperature with number of pulses for various laser beam incident angles (laser peak power = 15 MW, contaminant type = hydraulic oil, number of pulse = 20)

Figure 12 shows the effect of number of pulse on the ablation and thermal profiles. As seen, with a peak power of 30 MW the hydrocarbon based grease contaminants get removed even with ten laser pulses. Yttria particle starts to ablate after ten laser pulses and the complete 1.2 μm yttria particle is removed with 40 laser pulses and further increase in number of pulses starts to damage the substrate material.

4 Discussion

Laser cleaning of material can be defined as either the removal of particles or the removal of contaminant films from a solid surface [17]. The interaction of laser beam with materials is complex and an important phenomenon to be considered in any laser cleaning process. Typical mechanisms observed in laser cleaning of contaminants includes pure vaporization or decomposition [29], explosive removal caused by pressure build-up at the film-substrate interface [30] and two-phase removal induced by partial film vaporization and subsequent liquid expulsion [31]. Also, for the excimer laser pulse duration of 15–22 ns, melting and vaporization are mentioned to dominate the removal mechanisms [32].

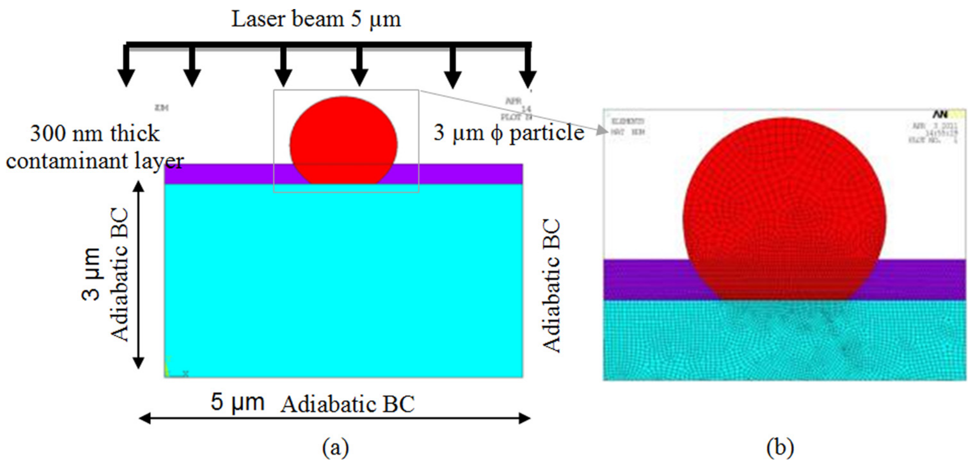

Fig. 10 Model domain and FEM mesh used for laser cleaning of contaminant layer with particles

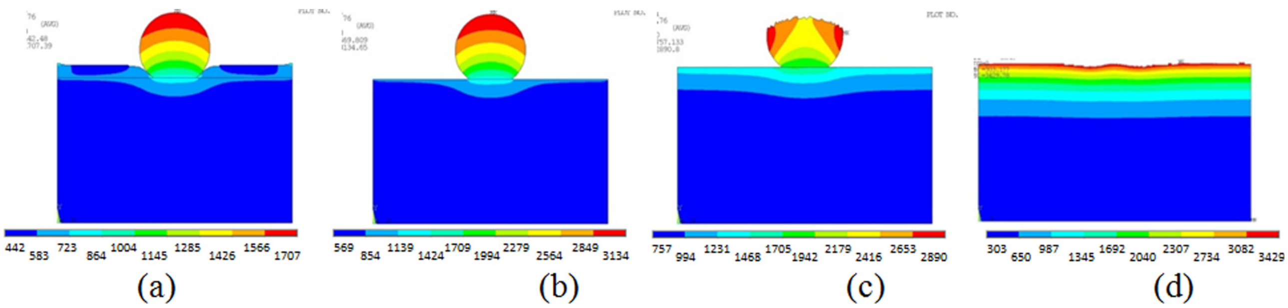

Fig. 11 Effect of laser peak power on temperature profile (K) and contaminant removal (contaminant type = yttria particle with grease layer, number of pulse = 20 and laser peak power: (*a*) = 10 MW, (*b*) = 15 MW, (*c*) = 30 MW, and (*d*) = 50 MW)

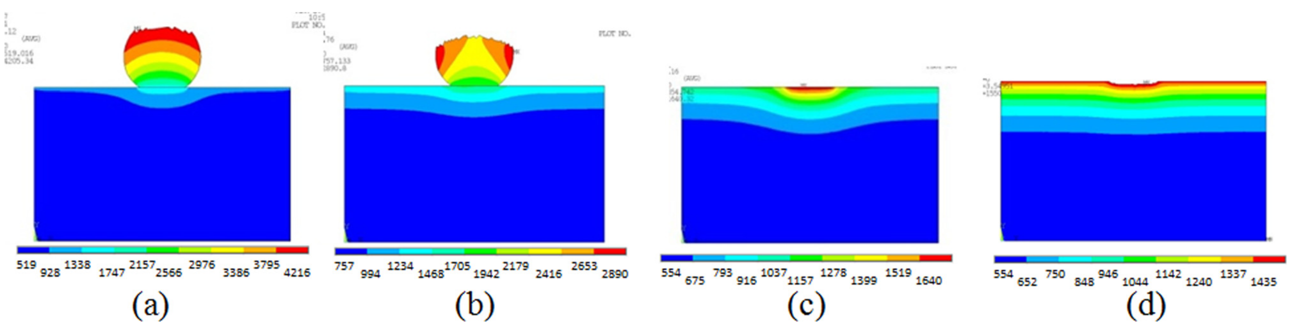

Fig. 12 Effect of number of pulses on temperature profile (K) and contaminant removal (contaminant type = yttria particle with grease layer, laser peak power = 30 MW and number of pulse: (*a*) = 10, (*b*) = 20, (*c*) = 40, and (*d*) = 60)

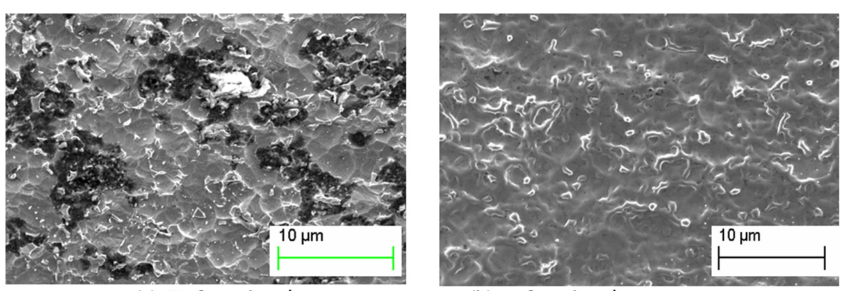

(a) Before cleaning (b) After cleaning

Fig. 13 Excimer laser cleaning of hydrocarbon based contaminants (peak power 15 MW, number of pulse = 20)

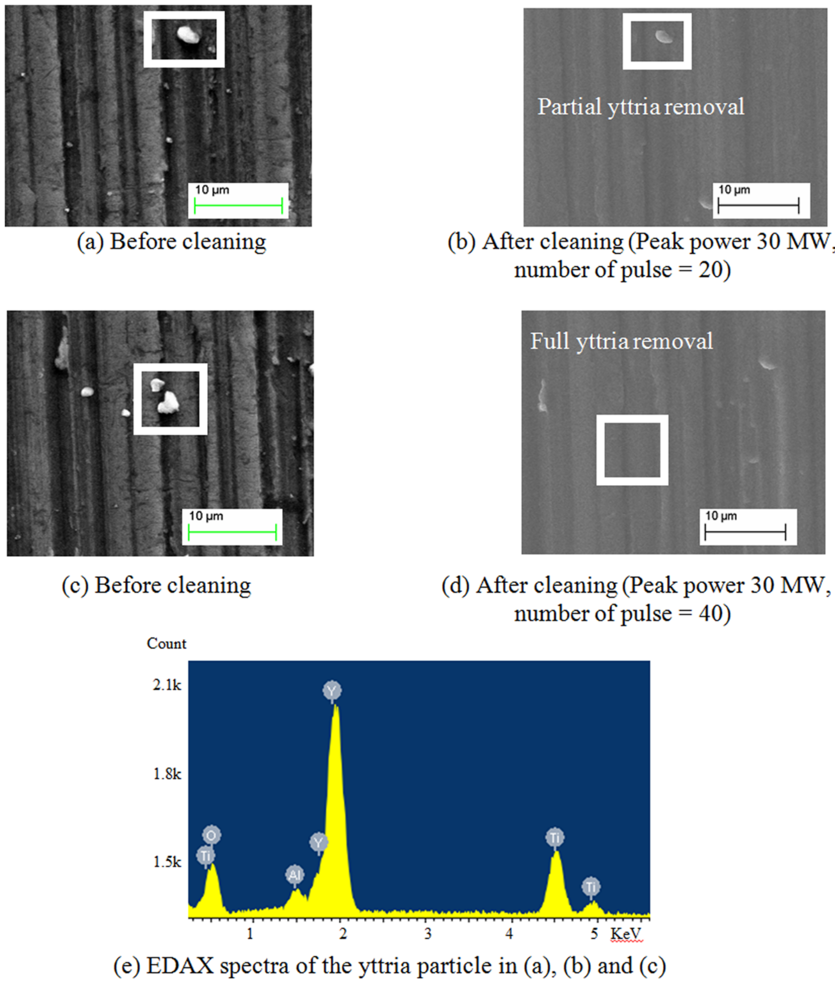

Fig. 14 Excimer laser cleaning of hydrocarbon and oxide based contaminants

Due to the low pulse duration of excimer laser, the commercially available temperature measuring devices cannot be used to obtain temperature information. The experimental validation is feasible only by comparing the surface ablation characteristic results obtained under similar process parameters.

Typical industrial based components primarily have hydrocarbon (hydraulic oil, grease) based contaminants and a very low fraction of oxides (yttria and magnesium oxide). As the hydrocarbon based contaminates have low boiling or decomposition temperatures they follow a vaporization/decomposition based removal mechanism. As noticed from Figs. 4–9, the surface temperature recorded is always higher than the decomposition temperature of hydrocarbon based contaminates which confirms the vaporization/decomposition as the possible removal mechanism. As shown in Fig. 13, the same phenomenon is found in the experimental observation as well. Figure 13(*a*) shows the sample before cleaning and Fig. 13(*b*) shows the same sample with cleaned surface for a laser peak power of 15 MW and 20 pulses. Furthermore, as seen in Fig. 7, the heating time in the excimer laser processing was on the order of ns and at this time period there will be little time for phase transformation and vaporization/decomposition may dominate for hydrocarbon based contaminants. The simulation suggests that the oxide based contaminants follows two-phase removal including partial melting and vaporization. As elucidated in Fig. 4, the top layer of the oxides gets ablated by vaporization but the surface temperature of the unablated oxides is higher than the melting temperature (2698 K) of yttria oxide. This suggests that the oxide layer removal mechanism follows partial melting and vaporization.

Figures 11 and 12 show that the effective removal of the yttria contaminants and hydro carbon based contaminants can be achieved with a laser peak power of 30 MW and 40 laser pulses. This observation was confirmed and also found in experimental samples as shown in Fig. 14. The SEM images in Figs. 14(*a*) and 14(*b*) show partial removal of yttria contaminate (at a peak power of 30 MW and 20 laser pulses) similar to the observation noticed in Fig. 12(*b*), whereas Figs. 14(*c*) and 14(*d*) shows complete removal of yttria contaminant at a peak power of 30 MW and 40 laser pulses contaminate similar to the observation noticed in Fig. 12(*c*). Figure 14(*e*) shows the elemental energy-dispersive

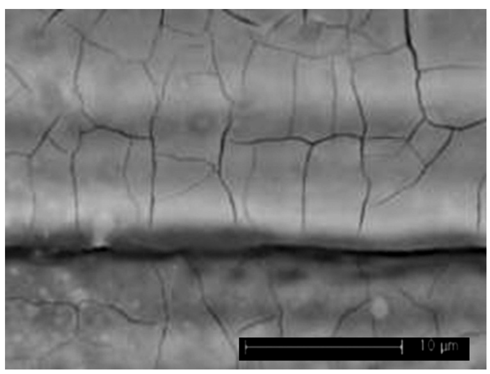

Fig. 15 Excimer laser cleaned sample (peak power = 40 MW, number of pulse = 80)

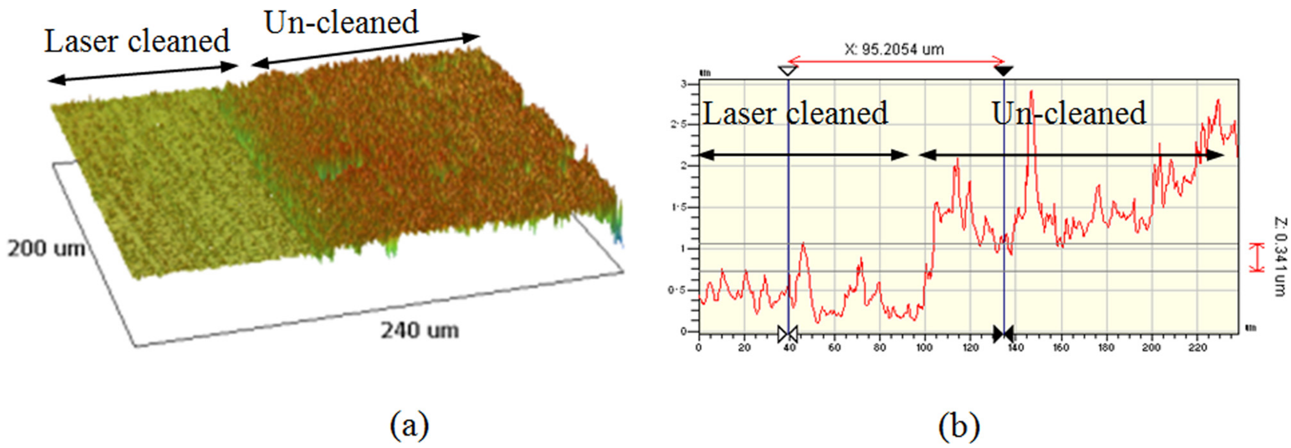

Fig. 16 3D surface topology and depth profile along laser cleaning interface (peak power = 15 MW, number of pulse = 20, contaminant type = grease)

X-ray spectroscopy (EDAX) spectra of the particle (inside the box) found in Figs. 14(*a*)–14(*c*), which shows high peak of yttria and oxygen. Similar to the simulation results of Fig. 12(*c*), the experimental observation at peak power of 30 MW and 40 laser pulses does not show any noticeable damage to the substrate. An increase in laser peak power and laser pulses (Figs. 11(*d*) and 12(d)) beyond the threshold range, results in melting and damage of the substrate material. Similar observations are noticed in the experimental results as shown in Fig. 15. With higher laser peak power and number of pulses, the contaminants are removed and also the top surface layer of the substrate gets melted. Once the laser beam is off, due to the rapid cooling cycle, the molten layer solidifies rapidly and gives rise to thermal solidification cracks as observed in Fig. 15.

Figure 16 shows the surface topology and the depth profile along the laser cleaned interface obtained using a white light interferometer (0.1 nm maximum resolution). The contaminant layer is of grease and the excimer laser cleaning was performed with a laser peak power of 15 MW and with 20 pulses. The experimental depth profile noticed in the Fig. 12(*b*) is very close to the FEM results shown in Fig. 8(*b*) performed under similar parameters.

Although both laser peak power and number of pulse have significant effect on laser cleaning efficiency, the laser peak power seems to be more sensitive and more significant. An increase in number of pulse from 20 to 40 increases the bulk temperature gradually to some extent (less than 5% as seen from Fig. 8) but an increase in peak power from 20 MW to 40 MW increase the temperature substantially (more than 50% as seen from Fig. 6) above the damage threshold temperature of the titanium substrate.

The thermal result of this FEM analysis gives a good insight of the ways and means to control the thermal damage of the material. Another important aspect that needs to be considered in any thermal process is the residual thermal stress in the material, caused due to the rapid heat and cooling cycle. Laser irradiation can induce thermal stress [33,34] on the material surface which can subsequently result in fatigue crack and other mechanical failures. To investigate the residual stress distribution in excimer laser cleaning process, a nonlinear thermostructural analysis was performed. The thermostructural analysis corresponds to the thermal analysis, with a peak power of 30 MW and number of pulse of 40 (Sec. 3.2; Fig. 12(*c*)). The mesh geometry used

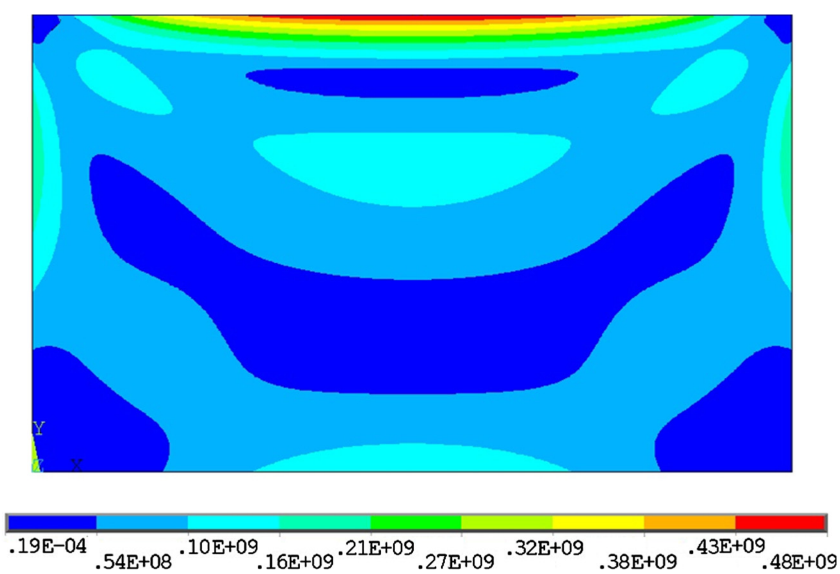

Fig. 17 Von Mises stress (Pa) distribution on laser cleaned substrate (peak power = 30 MW, contaminant type = yttria particle with grease layer, number of pulse = 40)

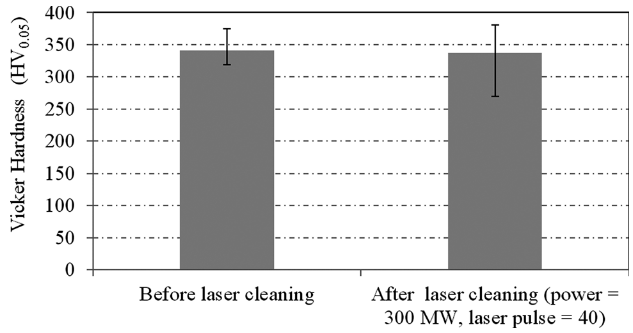

Fig. 18 Effect of laser cleaning on microhardness of the sample surface

for the thermostructural analysis is same as the one shown in Fig. 10. The thermal element of the mesh shown in Fig. 10 is replaced with the structural element type so as to perform the thermostructural analysis. The transient thermostructural investigation makes use of the temperature history predicted by the thermal analysis. Each time step in the thermostructural analysis corresponds to the time step in thermal analysis. During the thermostructural analysis, stress results are passed from one time step to the next time step as an initial stress condition; thereby maintaining the transient effects. Two edges (side) of the model (Fig. 10) were constrained along *X*-direction.

Figure 17 shows the von-misses stress distribution for peak power of 30 MW and for 40 pulses. This laser parameter seems to be the best combination of values as found from the thermal analysis. The plot in Fig. 16 shows only the substrates, as the contaminants have been ablated during the laser cleaning processing. As seen from the figure, the maximum stress distribution is found on the substrate surface just below the yttria particles. This is due to the enormous heat conducted from the yttria particle to the substrate. As the boiling temperature of the yttria particles is higher than substrate, yttria particles absorb enormous heat from the laser irradiation and conduct bulk of it to the substrate. The maximum stress distribution is close to 400 MPa which is less than half of the yield strength of the material, and another fact is that, noticeable stress distribution is found only in the first 0.1 μm from the surface which is of negligible thickness value compared to the thick bulk material. The microhardness of the material surface was experimentally evaluating using a Mitutoyo 5114 microhardness testing machine and shown in Fig. 18. As can be noted from the figure, the laser cleaning process at best parameter does not change the surface hardness level. Change in surface hardness can be used as clear indication [35] of the surface stress. An insignificant change of surface hardness was found in the experimental samples is in line with the surface stress values observed in Fig. 17.

5 Conclusions

The FEM model is capable of predicting the thermal profiles, ablation characteristic and stress distribution in excimer laser cleaning process. The thermal effect in the excimer laser processing (considering heating and cooling rates) on the substrate material is substantially low to create any thermal damages. The maximum stress distribution found on the substrate is substantially less than the yield stress of the material and it is found within negligible thickness from the substrate surface. The hydrocarbon based contaminants follow vaporization/decomposition dominated removal mechanism and the oxide based contaminates follow a partial melting and evaporation removal mechanism. The oxide based contaminates of 1.2 μm diameter required a minimum of 30 MW with 40 pulses to be fully removed. In excimer laser cleaning, laser peak power seems much more significant than the number of pulses.

Acknowledgment

The authors acknowledge the joint support offered by the UK Engineering and Physical Sciences Research Council (EPSRC) and the Technology Strategy Board (TSB) under the SAMULET Grant Nos. EP/G034745/1 and TP-AB265C/4, respectively.

References

[1] Turner, M., Crouse, P., and Li, L., 2006, "Laser Cleaning of Large Area Aerospace Components," Photon 06 Conference, Manchester, pp. 4–7.
[2] Kumar, A., and Gupta, M. C., 2009, "Surface Preparation of Ti-3al-2.5v Alloy Tubes for Welding Using a Fiber Laser," Opt. Lasers Eng., **47**(11), pp. 1259–1265.
[3] Kumar, A., Sapp, M., Vincelli, J., and Gupta, M. C., 2010, "A Study on Laser Cleaning and Pulsed Gas Tungsten Arc Welding of Ti-3al-2.5v Alloy Tubes," J. Mater. Process. Technol., **210**(1), pp. 64–71.
[4] Turner, M. W., Crouse, P. L., and Li, L., 2006, "Comparison of Mechanisms and Effects of Nd:Yag and Co2 Laser Cleaning of Titanium Alloys," Appl. Surf. Sci., **252**(13), pp. 4792–4797.
[5] Turner, M. W., Crouse, P. L., and Li, L., 2007, "Comparative Interaction Mechanisms for Different Laser Systems With Selected Materials on Titanium Alloys," Appl. Surf. Sci., **253**(19), pp. 7992–7997.
[6] Turner, M. W., Crouse, P. L., Li, L., and Smith, A. J. E., 2006, "Investigation Into Co2 Laser Cleaning of Titanium Alloys for Gas-Turbine Component Manufacture," Appl. Surf. Sci., **252**(13), pp. 4798–4802.
[7] Whitehead, D. J., Crouse, P. L., Schmidt, M. J. J., Li, L., Turner, M. W., and Smith, A. J. E., 2008, "Monitoring Laser Cleaning of Titanium Alloys by Probe Beam Reflection and Emission Spectroscopy," Appl. Phys. A: Mater. Sci. Process., **93**(1), pp. 123–127.
[8] Chen, G. X., Kwee, T. J., Tan, K. P., Choo, Y. S., and Hong, M. H., 2010, "Laser Cleaning of Steel for Paint Removal," Appl. Phys. A: Mater. Sci. Process., **101**(2), pp. 249–253.
[9] Garbacz, H., Fortuna, E., Marczak, J., Strzelec, M., Rycyk, A., Koss, A., Mróz, J., Zatorska, A., and Kurzydå, Owski, K. J., 2010, "Laser Cleaning of Copper Roofing Sheets Subjected to Long-Lasting Environmental Corrosion," Appl. Phys. A: Mater. Sci. Process., **100**(3), pp. 693–701.
[10] Song, W. D., Lu, Y., Hong, M., and Low, T., 1998, "Laser Cleaning of Magnetic Disks," Proc. SPIE, **3550**, p. 19.
[11] Zhou, X., Imasaki, K., Furukawa, H., Umino, H., Sakagishi, K., Nakai, S., and Yamanaka, C., 2001, "Simulation Study and Experiment on Laser-Ablation Surface Cleaning," Opt. Laser Technol., **33**(3), pp. 189–194.
[12] Furukawa, H., Nishihara, K., Yamanaka, C., Nakai, S., Imasaki, K., Zhou, X., Umino, H., Sakagishi, K., and Funahashi, S., 2000, "Laser Cleaning for Decontaminated Surfaces," Advanced High-Power Lasers and Applications, International Society for Optics and Photonics, pp. 128–136.
[13] Zhang, J., Wang, Y., Cheng, P., and Yao, Y. L., 2006, "Effect of Pulsing Parameters on Laser Ablative Cleaning of Copper Oxides," J. Appl. Phys., **99**(6), p. 064902.
[14] Tosto, S., 1999, "Modeling and Computer Simulation of Pulsed-Laser-Induced Ablation," Appl. Phys. A: Mater. Sci. Process., **68**(4), pp. 439–446.
[15] Oliveira, V., and Vilar, R., 2007, "Finite Element Simulation of Pulsed Laser Ablation of Titanium Carbide," Appl. Surf. Sci., **253**(19), pp. 7810–7814.
[16] Oliveira, V., Colaço, R., and Vilar, R., 2007, "Simulation of Krf Laser Ablation of Al2o3-Tic," Appl. Surf. Sci., **253**(18), pp. 7585–7590.
[17] Mullenix, N., and Povitsky, A., 2006, "Comparison of 1-D and 2-D Coupled Models of Gas Dynamics and Heat Transfer for the Laser Ablation of Carbon," J. Comput. Theor. Nanosci., **3**(4), pp. 513–524.
[18] Zinovik, I., and Povitsky, A., 2006, "Dynamics of Multiple Plumes in Laser Ablation: Modeling of the Shielding Effect," J. Appl. Phys., **100**(2), pp. 024911–024913.
[19] Sinha, S., 2010, "Nanosecond Laser Ablation of Thoria Fuel Pellets for Microstructural Study," J. Nucl. Mater., **396**(2–3), pp. 257–263.
[20] Khalil, A. a. I., and Sreenivasan, N., 2005, "Study of Experimental and Numerical Simulation of Laser Ablation in Stainless Steel," Laser Phys. Lett., **2**(9), pp. 445–451.
[21] Madenci, E., and Guven, I., 2006, *The Finite Element Method and Applications in Engineering Using Ansys*, Springer-Verlag, New York.
[22] Bogaerts, A., and Chen, Z., 2005, "Effect of Laser Parameters on Laser Ablation and Laser-Induced Plasma Formation: A Numerical Modeling Investigation," Spectrochim. Acta, Part B, **60**(9), pp. 1280–1307.
[23] Sobol, E. N., 1995, *Phase Transformations and Ablation in Laser-Treated Solids*, Wiley-Blackwell, New York.
[24] Georgiou, S., Zafiropulos, V., Anglos, D., Balas, C., Tornari, V., and Fotakis, C., 1998, "Excimer Laser Restoration of Painted Artworks: Procedures, Mechanisms and Effects," Appl. Surf. Sci., **127–129**, pp. 738–745.
[25] Wu, X., Sacher, E., and Meunier, M., 2000, "The Modeling of Excimer Laser Particle Removal From Hydrophilic Silicon Surfaces," J. Appl. Phys., **87**(8), p. 3618.
[26] Weast, R. C., Astle, M. J., and Beyer, W. H., 1988, *Crc Handbook of Chemistry and Physics*, CRC Press, Boca Raton, FL.
[27] Kanavin, A. P., Smetanin, I. V., Isakov, V. A., Afanasiev, Y. V., Chichkov, B. N., Wellegehausen, B., Nolte, S., Momma, C., and Tünnermann, A., 1998, "Heat Transport in Metals Irradiated by Ultrashort Laser Pulses," Phys. Rev. B, **57**(23), pp. 14698–14703.
[28] Chen, G., and Xu, X., 2001, "Experimental and 3D Finite Element Studies of Cw Laser Forming of Thin Stainless Steel Sheets," J. Manuf. Sci. Eng., **123**(1), pp. 66–73.

[29] Paek, U. C., and Kestenbaum, A., 1973, "Thermal Analysis of Thin-Film Micromachining With Lasers," J. Appl. Phys., **44**(5), pp. 2260–2268.
[30] Zaleckas, V. J., and Koo, J. C., 1977, "Thin-Film Machining by Laser-Induced Explosion," Appl. Phys. Lett., **31**(9), pp. 615–617.
[31] Veiko, V. P., Metev, S. M., Kaidanov, A. I., Libenson, M. N., and Jakovlev, E. B., 1980, "Two-Phase Mechanism of Laser-Induced Removal of Thin Absorbing Films. I. Theory," J. Phys. D: Appl. Phys., **13**(8), pp. 1565–1570.
[32] Miller, J. C., 1994, *Laser Ablation: Principles and Applications*, Springer, Berlin.
[33] Vikram, C. S., Pechersky, M. J., Feng, C., and Engelhaupt, D., 1996, "Residual-Stress Analysis by Local Laser Heating and Speckle-Correlation Interferometry," Exp. Tech., **20**(6), pp. 27–30.
[34] Cao, Y., Wang, Y., Dong, S., Yang, Y., Liang, Y., and Sun, T., 2007, "Residual Stresses around Femtosecond Laser Ablated Grooves in Silicon Wafer Evaluated by Nanoindentation," 3rd International Symposium on Advanced Optical Manufacturing and Testing Technologies, **6724**, p. 672417.
[35] Cerri, E., and Leo, P., 2011, "Mechanical Properties Evolution During Post-Welding-Heat Treatments of Double-Lap Friction Stir Welded Joints," Mater. Des., **32**(6), pp. 3465–3475.